Experiments in Fluids 33 (2002) 112–124
DOI 10.1007/s00348-002-0431-x

Time evolution of liquid drop impact onto solid, dry surfaces

R. Rioboo, M. Marengo, C. Tropea

Abstract The normal impact of liquid drops onto solid, dry surfaces has been studied experimentally, using high-resolution digital photography. A large number of parameters were varied in a systematic manner. The focus of this paper is the quantitative determination of the influence of these parameters on the drop spreading upon impact and on the phenomenological description of the outcomes. Dimensional similarity of the spreading can only be achieved for the very early stage of the impact process. At later stages, the number of influencing factors increases, generally precluding any universal correlation. Particular emphasis is placed on the influence of the wettability and the surface roughness on spreading.

1 Introduction

The impact of drops onto dry solid surfaces has been studied for over a century, not only because of the numerous physical phenomena of fundamental interest involved, but also due to its relevance in industrial applications (spray cooling, ink-jet printing, spray painting, fuel injection). Early studies of the impact process were largely phenomenological in nature, identifying the most important parameters influencing the spreading of the liquid film on the surface and also the final outcome of the impact. More recent studies and also the present study attempt to quantify the influence of individual parameters in order to obtain predictive capabilities of the impact process.

Before details and results of the present experiment are given, it is instructive to examine the schematic diagram shown in Fig. 1, which summarises the temporal development of the spreading film diameter after the instant of impact. The time t is made nondimensional using the impact velocity V and the initial spherical drop diameter $D(t^*=t(V/D))$. This particular way of making the time and the diameter nondimensional is usual for inertial driven impact and is justified by the different scales involved in the problem (see Schiaffino and Sonin 1997 for further methods of nondimensionalisation). The nondimensional diameter of the spreading film $d^*=d/D$ is often called the *spread factor*. The time evolution of the spread factor can be divided into four distinct phases: the kinematic phase, the spreading phase, a relaxation phase and a wetting/equilibrium phase.

This classification reflects observations from earlier studies, but it is expanded to also include results from the present study. The diverging lines in Fig. 1 are an arbitrary choice of possible outcomes, depending on the specific parameters of the impact process. One purpose of the present work is to establish under which conditions each phase occurs and the quantitative dependencies of the spread factor within each phase.

The experimental studies performed in this investigation have been restricted to drop impacts onto dry surfaces at a normal angle to the surface. Before continuing with a presentation of these results and their analysis, a brief review of previous work will be given.

In the first phase of impact and for high impact velocities, the liquid is compressed and a shock wave (spectacularly visualised in the works of Lesser and Field 1983; Dear and Field 1988; Field et al. 1985) is formed and detaches after reaching a critical angle. During this phase, the drop exhibits the shape of a cut sphere, derivable, as explained in Sect. 4, from purely geometric considerations of the impact. After this first phase, the spreading phase is characterised by the formation of a radially expanding film. As Worthington (1877a, 1877b) already showed, increasing the velocity sufficiently, leads to a splash. Furthermore, the *maximum diameter* achieved by the spreading film increases with the impact

Received: 31 July 2001 / Accepted: 26 February 2002
Published online: 15 May 2002

R. Rioboo (✉)
Université Mons-Hainaut,
Centre de Recherche en Modélisation Moléculaire,
Parc Initialis, Avenue Copernic,
7000 Mons, Belgium
E-mail: romain.rioboo@galileo.umh.ac.be
Tel.: +32-65373885

M. Marengo
Facoltà di Ingegneria,
Università di Bergamo, Viale Marconi 5,
24044 Dalmine, Italy

C. Tropea
Fachgebiet Strömungslehre und Aerodynamik,
Technische Universität Darmstadt,
Petersenstrasse 30,
64287 Darmstadt, Germany

The authors acknowledge financial support of the Deutsche Forschungsgemeinschaft through grant Tr 194/12 (Strategic grant program "Wetting and Structure Formation at Interfaces"), the German–Israeli Foundation through Grant No. I-536–97.14/97 and the DAAD-CRUI VIGONI Program for scientific exchange between Germany and Italy. The authors are also grateful for scientific discussions and collaborations with Dr. Daniel A. Weiss, Sefko Sikalo, and particularly with Dr I.V. Roisman.

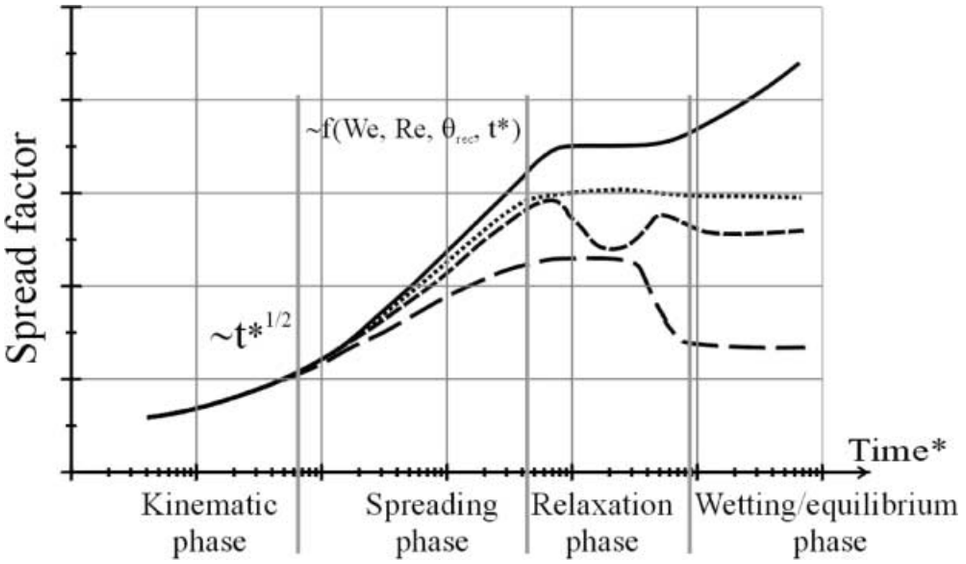

Fig. 1. Schematic representation of the spread factor with time. The different lines correspond to an arbitrary choice of possible spreading histories, depending on the parameters of the impact

velocity (Levin and Hobbs 1971; Cheng 1977; Fukai et al. 1995). Levin and Hobbs (1971) showed that the ratio between the spreading velocity and the impact velocity diminishes as the impact velocity increases. Nevertheless, the amount of data on which this statement is based and the time resolution of their image acquisition system (0.1 ms) may explain differences with the results presented in Sect. 3. Several authors (Prunet-Foch et al. 1998; Mourougou-Candoni et al. 1997; Zhang and Basaran 1997) studied the effect of surfactants on the spreading and recoil of a drop. The maximum spreading radius of surfactant-laden drops is smaller than with water drops when the impact velocity becomes high enough. The surfactant appears to stabilise the wave motion during the recoil phase.

As remarked by Engel (1955), surface roughness influences the phenomenon of the impact. She noticed that with rough surfaces, splashing occurs for less energetic impacts than polished surfaces, as confirmed by Levin and Hobbs (1971). Hartley and Brunskill (1958) found that a necessary condition to obtain droplet rebound was the presence of 'micro-roughness' on the leaves of the plants that were investigated. Stow and Hadfield (1981) were the first to make a systematic study of the roughness amplitude. Most empirical correlations describing the influence of roughness on the splash threshold have been established with a limited number of surface and liquid variations, and, in the authors' experience, it is not difficult to find contradictions when other materials are used. This is presumably due to wettability effects, as also was speculated by Range (1995), and indeed, was one of the motivations for the present work.

The influence of the wettability of the system (solid–liquid–gas) had been visualised already by Worthington (1877a). Hartley and Brunskill (1958) showed the importance of this parameter to obtain a rebound of the droplets after impact onto leaves. They included in the lamella energy balance, the spreading energy, which includes the usual wetting parameter, the static contact angle. Podvysotskii and Shraiber (1993) found that at high impact velocities the wettability has much less of an influence on the deposition rate than the roughness.

2 Experimental set-up

An experimental set-up was constructed to allow the impact of single droplets onto a defined surface, to be studied with high temporal and spatial resolution. Figure 2 shows the experimental set-up.

The drop is generated using a precision syringe (Hamilton Samplelock syringe and RN needles of different diameters). The drop diameter is dependent on the diameter of the syringe needle, which can be varied from 0.15 to 3.5 mm. For slightly nonspherical drops an equivalent drop diameter $D_{eq} = \left(D_{hori}^2 D_{vert}\right)^{1/3}$, can be defined, where diameters D_{hori} and D_{vert} are the horizontal and vertical diameters of the ellipsoidal image of the ovoid drop, respectively. The drop falls from a predetermined height, which also defines the impact velocity, and triggers, by means of a light barrier, an electronic delayer used to

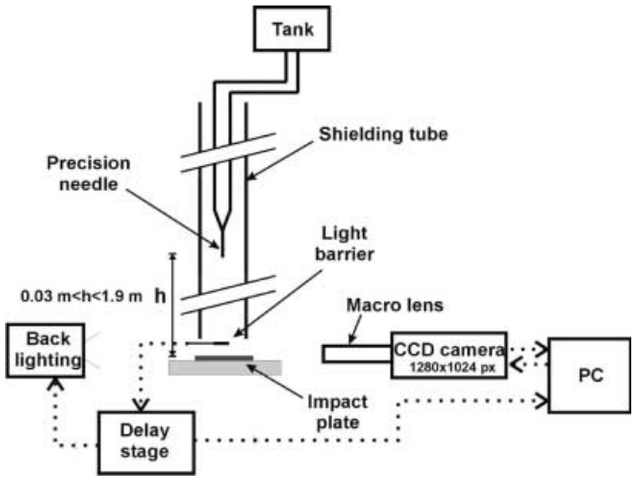

Fig. 2. Experimental set-up

synchronise the stroboscope and the camera. The repeatability of the drop generation and its trajectory is extremely high, so that the entire impact process can be highly resolved in time by choosing different delay phases for each repeated experiment. The excellent repeatability is achieved by using Teflon-coated needles or by coating the needles with wax. In order to verify the reproducibility during the impact process, five pictures were taken for each selected time of the event. During the processing of the data, the lamella diameter was measured and a quantitative evaluation of the reproducibility was made. The standard deviation of the measured diameter over five images was always under 3%. Only the final stages of recoil, when using highly nonwettable surfaces, were observed to be less repeatable.

The images were captured using a high-resolution (1280×1024 pixels) CCD camera (Sensicam, PCO), capable of acquiring up to ten multiple exposures. Multiple exposures were taken with a continuous light source and were used only when the precise time of impact had to be determined. In this case the exposure time and the time between exposures were chosen to capture at least two images of the droplet before impact and up to eight images after impact. Such a multiply exposed image is shown in Fig. 3a. Both the exposure times and exposure delays could be individually varied for all ten exposures between 100 ns and 1 ms. From a set of at least five such images, the impact velocity and the instant of impact were estimated. The velocity was estimated using a linear interpolation between two images and the instant of impact was estimated using a linear extrapolation of the last two images before impact. For instance, in Fig. 3b the first image after impact is estimated to be at t=20 μs. Especially for studying the early impact stage, the determination of the instant of first contact represents the single largest source of relative error. An uncertainty analysis on the impact time has been performed and error bars corresponding to 95% (two standard deviations) confidence have been added to the presentation of results where appropriate.

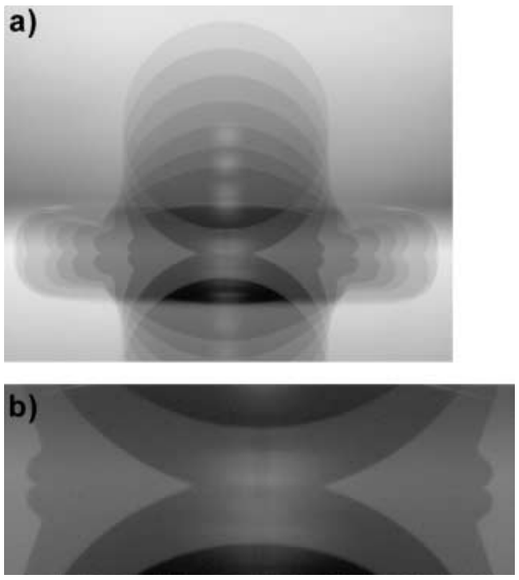

Fig. 3a, b. Impact of a 2.73-mm diameter drop of glycerine at 10 cS on a glass surface at 0.96 m/s, time between exposures was 365 μs: **a** the whole drop; **b** zoom on the two first exposures after impact

For later stages of spreading, the impact instant in terms of delay since the light barrier trigger was then assumed to be known. For a given delay time, adjustable using the electronic delayer, single-frame images were acquired using a xenon strobe lamp with a flash duration of 3 μs. The shutter exposure time was 1 ms, thus the flash was the determining factor in illumination.

Table 1 provides an overview of all the parameters that were varied and their ranges. The liquids used were acetone, isopropanol, ethanol, water, silicone oils and mixtures of glycerine and water. The solid surfaces used were glasses, PVC, wax, polymer coatings (a commercial product RainX, Quaker State) and AKD (alkylketene dimer as in Onda et al. 1996).

The wettability of each surface was characterised by measuring the static contact angle using the sessile drop method (Johnson and Dettre 1993). With this method both an advancing (θ_{adv}) and receding (θ_{rec}) contact angle can be obtained, in this particular case with a precision of ±3°. However, these angles still refer to the static contact angles in the sense that the velocity of the contact line is practically zero. At nonzero velocities the advancing and receding contact angles differ from their static values, generally as a function of the capillary number (Hoffman 1975). The difference between the advancing and receding contact angles at zero velocity is the hysteresis, attributed to chemical or topological inhomogeneities (de Gennes 1985). The classical static contact angle defined by Young's equation will lie between θ_{adv} and θ_{rec}.

The roughness parameter R_z expresses the mean absolute deviation from a flat surface as defined according to the codes DIN 4768 and DIN ISO 1302. The value of R_z is determined by taking a segment of the surface contour line, dividing it into five equal parts and then averaging the maximum amplitude found on each of the five sub-segments. For some surfaces, a roughness wavelength (R_w) is defined. This refers to the case of a square pattern of pyramids on the surface of the solid plate, created using excimer laser ablation. The value of the wavelength is the distance between two adjacent peaks. The height of the pyramids was 5 μm.

Table 1. Experimental parameters

Parameters studied	D (mm)	V (m/s)	σ (kg/m^2)	μ (kg/ms)	R_a (μm)	R_w (μm)	θ_{adv} (°)	θ_{rec} (°)
Min.	1.2	0.78	0.021	0.3 10^{-3}	0.003	100	0	0
Max.	4.9	4.1	0.073	934 10^{-3}	120	1000	162	154

Great care was taken in cleaning the surfaces. In most of the cases, ethanol and acetone were used. To achieve complete wetting on glass, sulfochromic acid was used as a cleaning agent. In this case, the static contact angle with distilled water was zero. To remove silicone oil drops, methyl ethyl ketone was used. The quality of cleaning was periodically checked by performing contact angle measurements.

3
Experimental observations

All spreading curves appear to have different stages (Fig. 1). The first stage represents the *kinematic phase*, when the dimensionless contact diameter increases with approximately $t^{*0.5}$, followed by a *spreading phase* where all the other parameters begin to play a role in the impact evolution. The spreading phase is followed by a *relaxation phase*, which may have different outcomes, depending mainly on the magnitude of the receding contact angle. In a final phase, the lamella decelerates strongly and attains some constant diameter (*equilibrium phase*) or, for highly wettable surfaces, continues slowly to wet the surface (*wetting phase*).

3.1
Kinematic phase

At the early stage of impact, the shape of the drop resembles a truncated sphere. During this phase no spreading lamella is yet visible. Figure 4 shows the time evolution of the dimensionless spreading diameter for various cases and for nondimensional times $t^*<0.1$. The diameter grows according to a power law in time, with an exponent lying between 0.45 and 0.57. The main experimental uncertainty lies not in the diameter measurement but in the time measurement, since the exact instant of impact must be interpolated between two exposures. At the dimensionless time of $t^*=0.003$ the contact diameter uncertainty is about ±7% (95% confidence), whereas the time uncertainty is about ±25% (95% confidence). The time uncertainty reduces dramatically for larger values of t^*, as indicated by the two example "error bars" included in Fig. 4. For example, at $t^*=0.1$ the uncertainties are ±1% in t^* and ±6.5% in d^*, respectively. In the kinematic phase, the wettability is not influential, as indicated in Fig. 5. Also no difference can be seen in the overall shape of the drop throughout this initial phase.

Together, Figs. 4 and 5 provide a comprehensive picture of the drop spreading at very small dimensionless times $t^*<0.1$. It is clear from this systematic variation of numerous parameters that this phase of the impact process is completely described by the impact velocity and initial diameter.

3.2
Spreading phase

With increasing time, a lamella is ejected from the base of the drop and forms a thin film bounded by a rim. Figure 6 shows the spreading phase of this lamella for five different cases, all impacting onto glass (the system wettability is still of little influence in this stage). The 2.64-mm drop of glycerine (100 cS) impacting at 0.96 m/s has been used as a reference case and each subsequent case varies one single

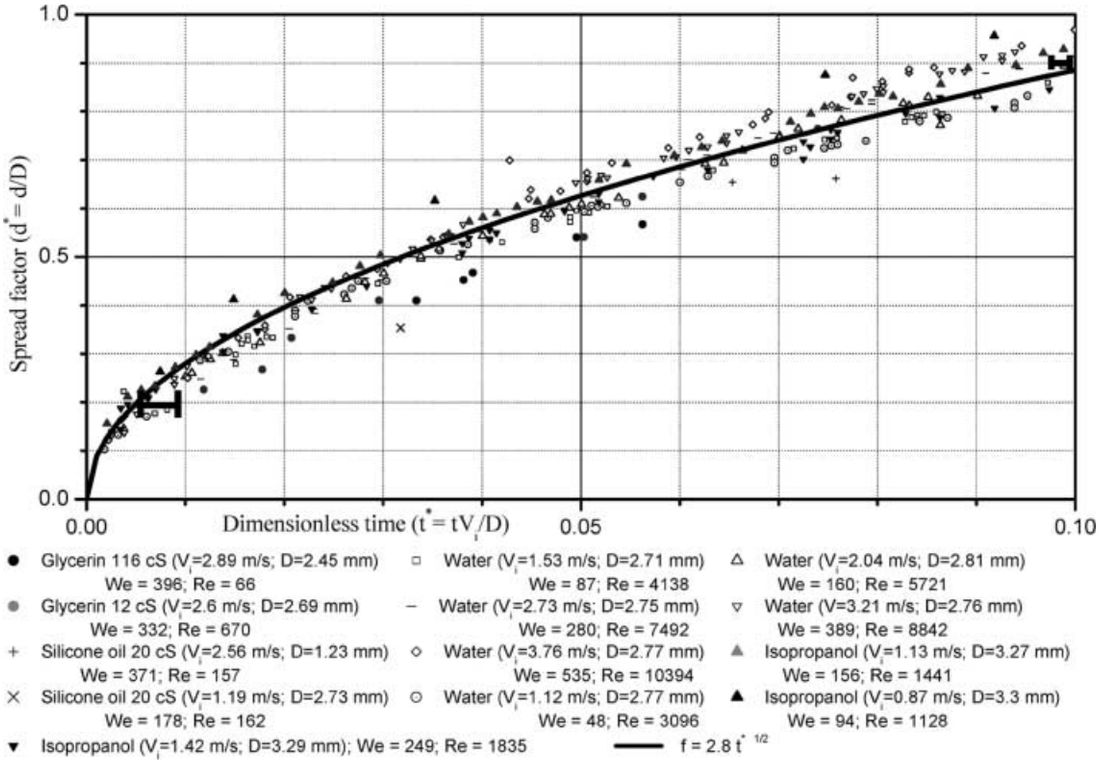

Fig. 4. Spread factor of liquid drops of various diameters and impact velocities on a glass surface

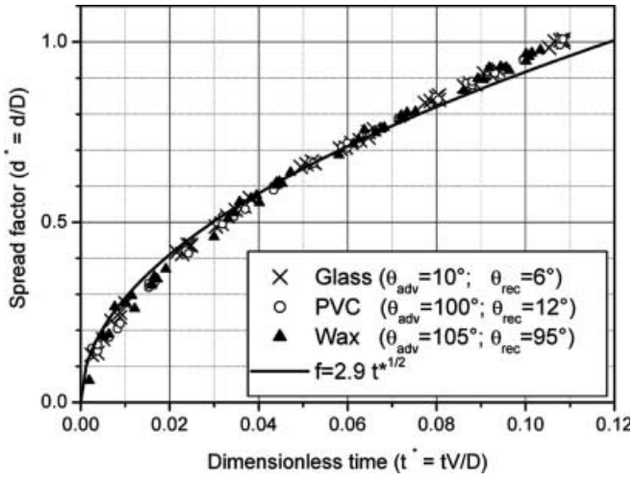

Fig. 5. Spread factor as a function of dimensionless time for *We*=390. Impact conditions for the liquid were constant: water drop, impact velocity *V*=3.21 m/s, drop diameter *D*=2.76 mm. The solid surfaces were changed: glass (θ_{adv}=10°, θ_{rec}=6°); wax (θ_{adv}=105°, θ_{rec}=95°); PVC (θ_{adv}=100°, θ_{rec}=12°)

parameter: surface tension, viscosity, diameter or velocity. Bars indicating the uncertainty in time and spreading diameter have been added for one low and one high (0.8) value of t^* on the silicone oil curve.

The results confirm many influences discussed in the literature and indeed confirm first expectations: increasing the impact velocity or drop diameter leads to faster spreading, and increasing the surface tension or viscosity leads to slower expansion. Once the lamella is formed, similarity is no longer achieved using simply dimensionless diameter and time. Understandably, the influence of surface tension and viscosity cannot be accounted for just with the dimensionless time, however, it is of particular interest that also the drop diameter and impact velocity after t^*=0.1 are quite influential and cause a change in the behaviour of the spreading law. The surface tension seems to be of little influence until $t^* \cong 0.5$, but for $0.5 < t^* < 2$ the spreading diameter increases by 10% when the surface tension is reduced by a factor of 3.

Figure 7 shows in more detail the influence of the drop diameter. The 4.9-mm drop results in a spreading diameter much larger than the other two (2.7 mm). Superficially, this also suggests that the drop volume must be considered. It should be remarked, however, that in this apparatus large droplets still exhibit some residual oscillations upon impact, arising from the drop generation process. The smallest observed aspect ratio was, for instance, 0.76. The exact shape of the droplet upon impact will definitely influence the initial kinematic phase and can possibly explain abnormally high spreading diameters for very small times, as observed in Fig. 7. Such flattening effects can be expected to be particularly important for large drops and low impact velocities (Middleman 1995; Frohn and Roth 2000).

In Fig. 8 the spreading evolution as a function of viscosity is shown ($V/D \approx 1$, D is held constant). Viscosity clearly influences the spreading diameter and its effect increases with time. It can be seen that the *maximum diameter* is smaller and is reached earlier when the viscosity increases.

Also of primary interest is the influence of the impact velocity on the spreading diameter, as shown in Fig. 9. As with the drop diameter, a simple dimensionless time does not lead to similarity in the diameter evolution. Increasing the impact velocity will increase the dimensionless spreading diameter for a defined t^* (30% more for a factor of 2 in velocity and 60% more for a factor of 2.7).

Wettability is of no influence during the *kinematic phase*, but as the time increases its effect can be important,

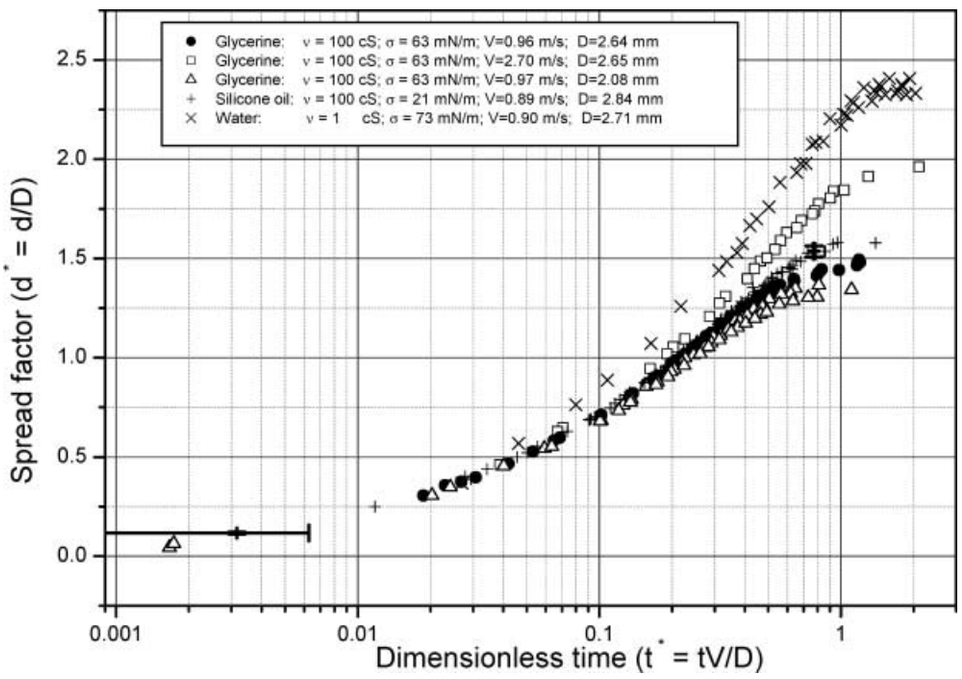

Fig. 6. Spreading phase of various drop impacts

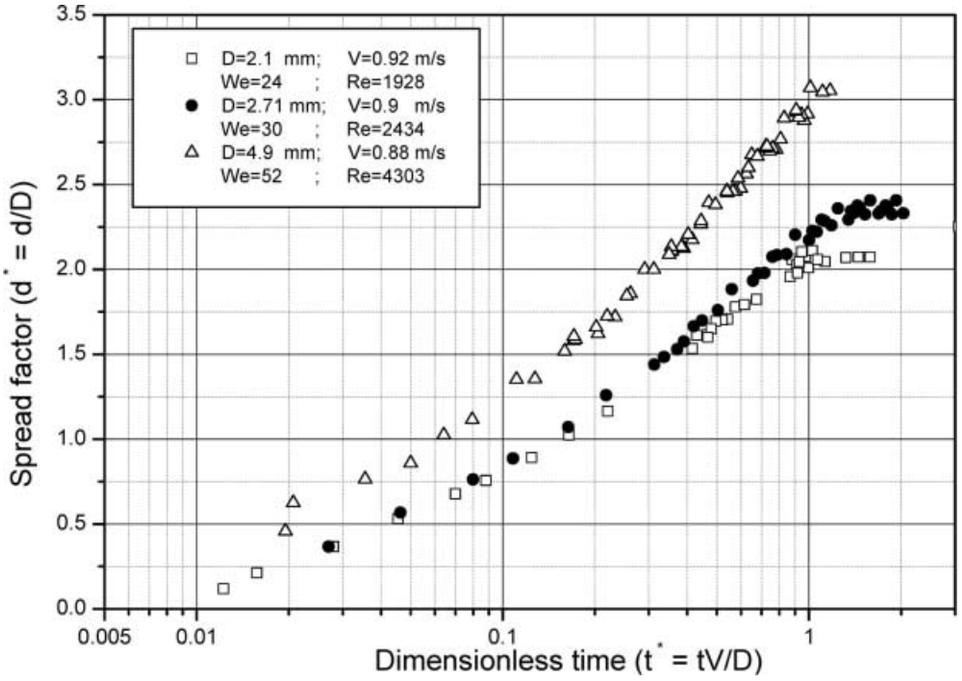

Fig. 7. Drop diameter influence on the spreading factor for water drops impacting on glass

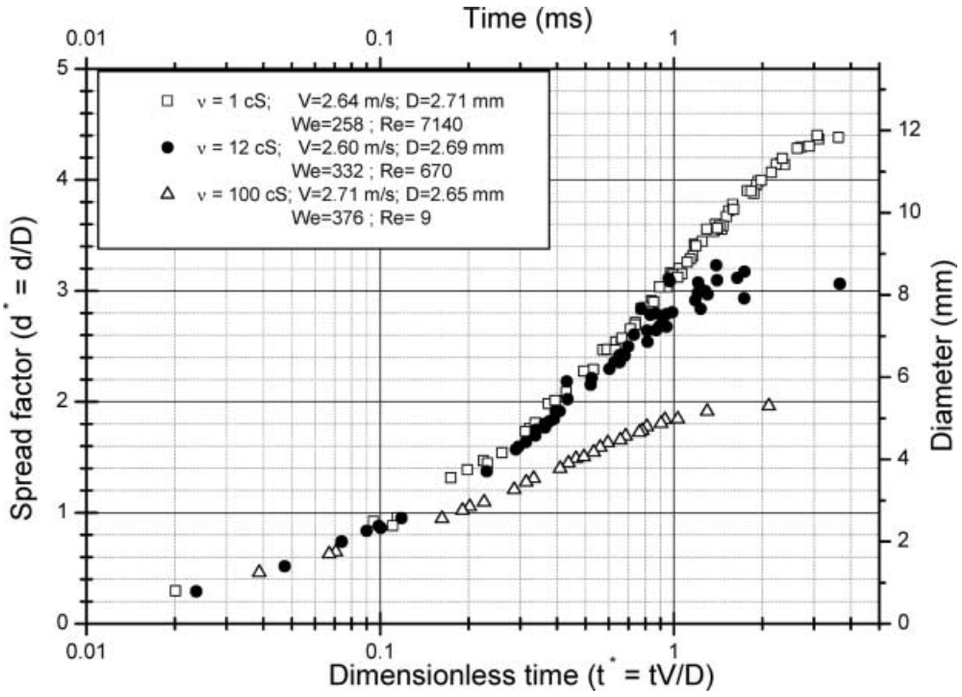

Fig. 8. Influence of the viscosity on the spreading diameter in time. Dimensional and dimensionless forms can be seen on the same graph since *V*/*D* is held constant

as illustrated in Fig. 10. During most of the spreading, the three curves behave in the same way. Only in the final phase, at dimensionless times $t^*>2$, is a difference discernible for the water-repellent case (θ_{rec}=154°). The drop comes to rest earlier and with a smaller maximum diameter. There is only a very slight difference between the case of almost wettable (θ_{rec}=6°) and partially wettable (θ_{rec}=86°) surfaces. It was possible to measure the dynamic contact angle during the spreading, and in the case of the repellent surface, it never fell below 130°. For the RainX-coated glass plate (with θ_{rec}=86°), the dynamic contact angle decreased to 90° at times above about 6 ms. Note that in Fig. 10 the receding contact angle has been listed in the caption, although the film is increasing in diameter. This is because the receding contact angle is later shown to be the quantity that determines the maximum spread diameter and the behaviour of the film afterwards.

These results stand both in agreement and in contradiction to previous studies. Fukai et al. (1995) have

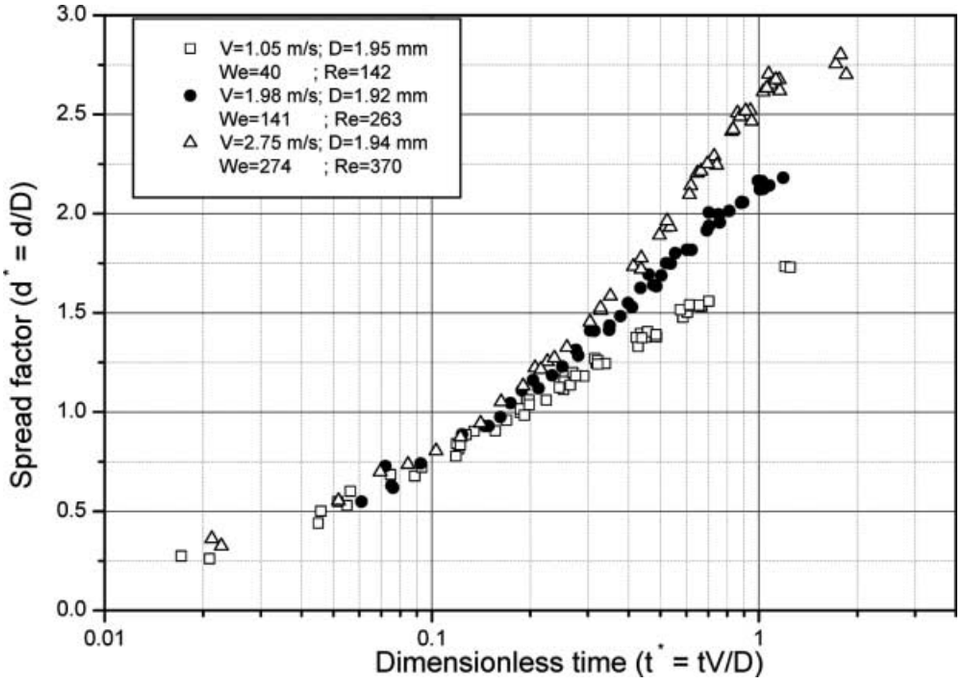

Fig. 9. Influence of the impact velocity in dimensional and dimensionless form for glycerine at 20 cS

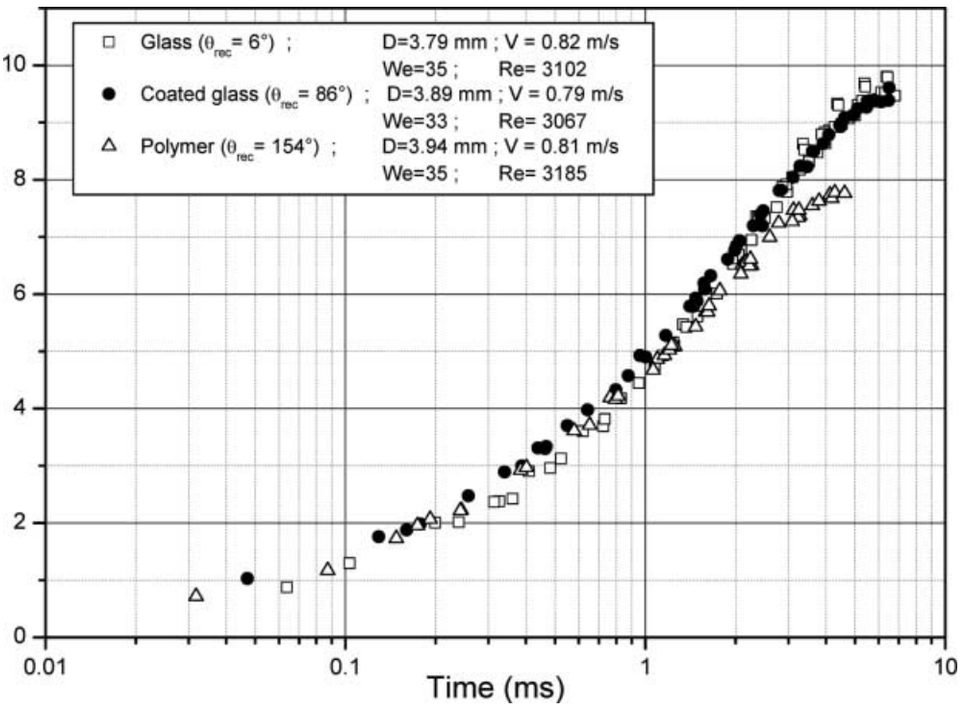

Fig. 10. Wettability influence on the spreading behaviour. All experiments were performed with water; drop sizes and velocities are comparable

demonstrated numerically and experimentally that wettability is influential throughout the entire spreading phase. On the other hand, Richard (2000) and Mao et al. (1997) have observed no difference in maximum spreading diameter while changing the static contact angles. In the present case, differences are only observed for very hydrophobic conditions and only during the final stage of spreading.

If the wetting effects are considered secondary throughout most of the spreading phase, the drop evolution in time should be described by nondimensional parameters, including the factors viscosity, surface tension, drop diameter and impact velocity. Thus the Reynolds number and Weber number should be appropriate, expressing the ratios of momentum to viscous and momentum to capillary forces. In Fig. 11 the influence of the Reynolds number on the spreading diameter is shown, while keeping the Weber number constant at two different values.

Different liquids with different impact conditions were used intentionally in each of these two diagrams.

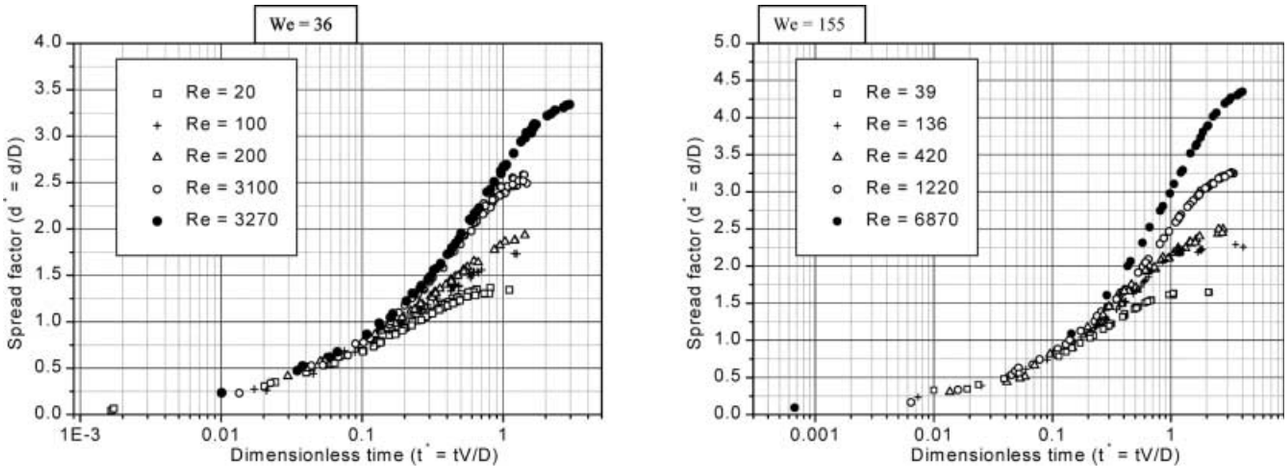

Fig. 11. Influence of Reynolds number on the spread factor; the Weber number is kept constant (*We*=36, *left*; *We*=155, *right*)

Evidently, increasing the Reynolds number leads to an increase in the spreading diameter. Of particular interest is the comparison of the two curves: *We*=36, *Re*=3,270 and *We*=36, *Re*=3,100. In spite of the fact that the Weber and Reynolds numbers are very close, the drop shows clear differences in its spreading for $t^*>1$. In this particular case, water (*Re*=3100) and acetone (*Re*=3270) were used. The difference in spreading cannot be attributed to wettability effects, since all experiments were performed with glass as a target surface and, as Fig. 10 indicates, no effects are expected until very high static contact angles are reached. Also of particular interest is the fact that, for example, taking *Re*=39 and *Re*=136 (with a ratio of 3.5 between Reynolds numbers), the nondimensional diameter d^* is increased by 35%, while between *Re*=136 and *Re*=420 d^* it is increased by only 10% and between *Re*=420 and *Re*=1220 d^* it is increased by 30%. This diameter ratio shows a nonlinear and nonmonotonic behaviour with the Reynolds number.

The influence of the Weber number is weaker and can be seen in Fig. 12, for which the Reynolds number was held constant at *Re*=192. An increase of 20% is observed for d^* when the Weber number is increased by a factor of 3.7 for a given time t^* (t^*=1, for example). This confirms the role of surface tension during the latter stages of spreading. A further increase in the Weber number can be obtained by increasing the impact velocity and using low surface tension liquids. But in that case, the lamella detaches from the solid surface, resulting in a rim break-up, ejected droplets or possibly the formation of a corona (Rioboo et al. 2001).

During all the phases of the spreading, including the first kinematic phase, the contact diameter is decelerating. This is not immediately evident from the logarithmic plots used to show the results, but is very evident from linear plots.

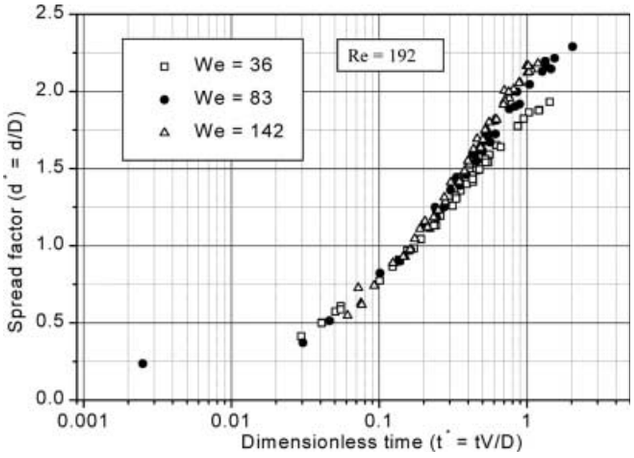

Fig. 12. Influence of the Weber number on the spread factor (*Re*=192)

3.3 Relaxation phase

After the spread phase the drop may begin to recede. This is illustrated in some of the sequences shown in Fig. 13 of water droplets impacting onto three different surfaces. The roughness of each surface and the impact velocity were both varied between two values such that the various influencing parameters could be studied separately. The exact experimental conditions are listed in Table 2 and of the 12 parameter combinations, 8 have been highlighted in Fig. 13.

Comparing the wax sequences (θ_{rec}=95° or 85° for the rough surface) with those of glass (θ_{rec}=6° or 16° for the rough surface) and PVC (θ_{rec}=12° or 19° for the rough surface), a receding motion is found only for the wax surface. The only parameter that is significantly different in this case is the receding contact angle. Another feature that can be seen from these experiments is the influence of the roughness amplitude. For impacts at low velocity on rough surfaces, perturbations on the rim appear (for example, wax, low impact velocity, *t*=3.15 ms; glass, low impact velocity, *t*=2.27 ms and *t*=3.15 ms). At high impact velocities the perturbations of the rim are already present even on smooth surfaces. On rough glass at high impact velocity, a prompt splash (Rioboo et al. 2001) occurs, where filaments of droplets are ejected (*t*=0.86 ms,

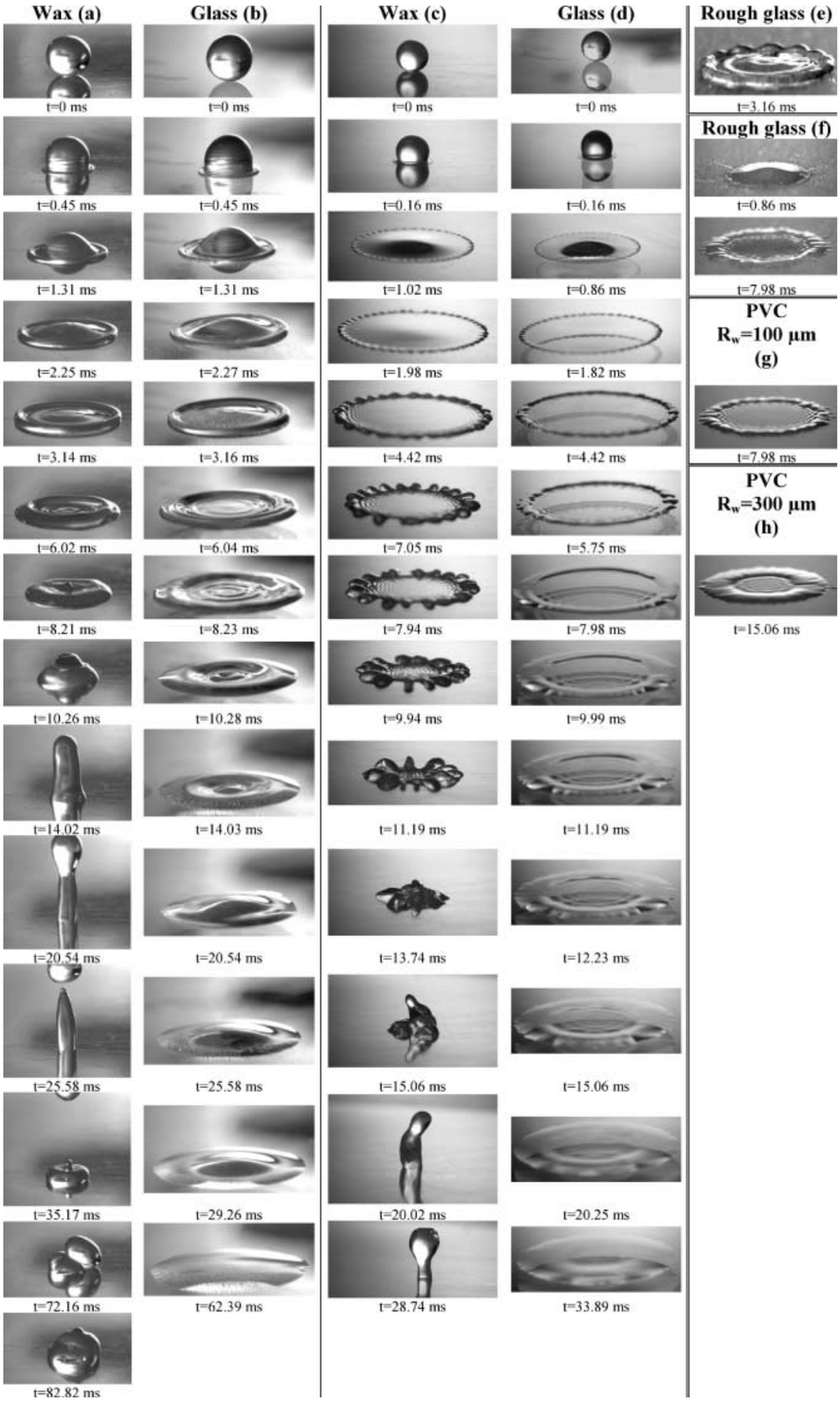
Wax (a)
Glass (b)
Wax (c)
Glass (d)
Rough glass (e)
Rough glass (f)
PVC
R_w=100 µm
(g)
PVC
R_w=300 µm
(h)
t=0 ms
t=0 ms
t=0 ms
t=0 ms
t=3.16 ms
t=0.45 ms
t=0.45 ms
t=0.16 ms
t=0.16 ms
t=0.86 ms
t=1.31 ms
t=1.31 ms
t=1.02 ms
t=0.86 ms
t=7.98 ms
t=2.25 ms
t=2.27 ms
t=1.98 ms
t=1.82 ms
t=3.14 ms
t=3.16 ms
t=4.42 ms
t=4.42 ms
t=7.98 ms
t=6.02 ms
t=6.04 ms
t=7.05 ms
t=5.75 ms
t=8.21 ms
t=8.23 ms
t=7.94 ms
t=7.98 ms
t=15.06 ms
t=10.26 ms
t=10.28 ms
t=9.94 ms
t=9.99 ms
t=14.02 ms
t=14.03 ms
t=11.19 ms
t=11.19 ms
t=20.54 ms
t=20.54 ms
t=13.74 ms
t=12.23 ms
t=25.58 ms
t=25.58 ms
t=15.06 ms
t=15.06 ms
t=35.17 ms
t=29.26 ms
t=20.02 ms
t=20.25 ms
t=72.16 ms
t=62.39 ms
t=28.74 ms
t=33.89 ms
t=82.82 ms

◄

Fig. 13a–h. Sequences of water drop impacts: **a** wax: V_i=1.18 m/s, R_a=0.4 μm; **b** glass: V_i=1.18 m/s, R_a=0.003 μm; **c** wax: V_i=3.6 m/s, R_a=0.4 μm; **d** glass: V_i=3.6 m/s, R_a=0.003 μm; **e** glass: V_i=1.18 m/s, R_a=3.6 μm; **f** glass: V_i=3.6 m/s, R_a=3.6 μm; **g** PVC: V_i=3.62 m/s, R_w=100 μm; **h** glass: V_i=3.62 m/s, R_w=300 μm (see Table 2 for further details)

t^*=0.91). This is seen neither on the smooth glass plate nor on the rough wax, despite the fact that the roughness amplitude is higher than that of the rough glass.

The PVC sequences show no significant differences caused by the change of roughness wavelength (100 and 300 μm) at either high or low impact velocities. Considering separately the high and low impact velocity sequences, it is seen that during the spreading phase the shape of the drop is very similar for all surfaces. However, for the high velocity impact onto a rough surface, a prompt splash changes the phenomenology. In this case, after the splash, the shape of the spreading drop is comparable to a drop impacting onto a smooth glass surface. From the sequences on wax, the perturbations along the rim merge continuously during the receding process until the liquid rises vertically (at maximum diameter the number of lobes is 47 at t=2 ms, and their number decreases to 8 at t=12 ms). A partial rebound is then observed, with a small time shift between the smooth (t≈25.6 ms) and rough (t≈27 ms) surfaces. This small delay between partial rebounds on smooth and rough surfaces was also present in the spreading diameter curves shown in Fig. 14, which summarises the spread factors measured from sequences partially presented in Fig. 13. At high impact velocities onto wax, however, the partial rebound was not always observed. The reproducibility of the process following the receding stage was not high, i.e. whether the liquid was ejected from the surface or not. Usually one or even two droplets were observed, but, as observed by Rioboo et al. (2001), secondary droplets were sometimes left on the surface during the receding motion (receding break-up), and in that case no partial rebound occurred.

3.4 Wetting/equilibrium phase

All the previous sequences, even the ones for glass surfaces, were performed under conditions of partial wetting (θ_{adv}>0). In contrast, Fig. 15 shows the time evolution for

Table 2. Experimental conditions

Material	Glass		Wax		PVC	
Wettability with water (θ_{adv}, θ_{rec})	10°, 6°	78°, 16°	105°, 95°	105°, 85°	100°, 12°	90°, 19°
Roughness amplitude (μm)	0.003	3.6	0.4	25.6	6.2	6.2
Roughness characteristic wavelength (μm)	–	–	–	–	300	100
Drop diameter (mm)	3.04, 3.17	3.03, 3.17	2.75, 3.17	3, 3.17	2.65, 3.42	2.65, 3.42
Impact velocity (m/s)	1.18, 3.6	1.18, 3.6	1.18, 3.6	1.18, 3.6	1.22, 3.62	1.22, 3.62
Weber number	58, 563	58, 563	52, 563	57, 563	54, 614	54, 614

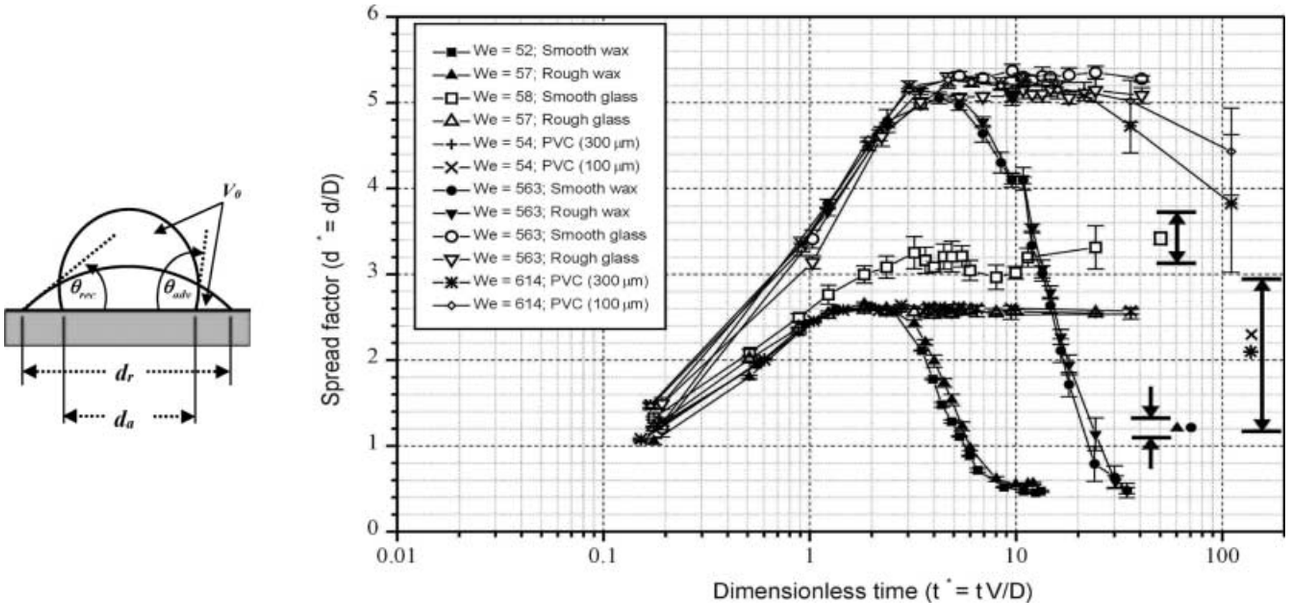

Fig. 14. Time evolution of the spread factor for a water drop impact onto various surfaces (*right*, see Table 2 for specifications); sketch of equilibrium diameters (*left*)

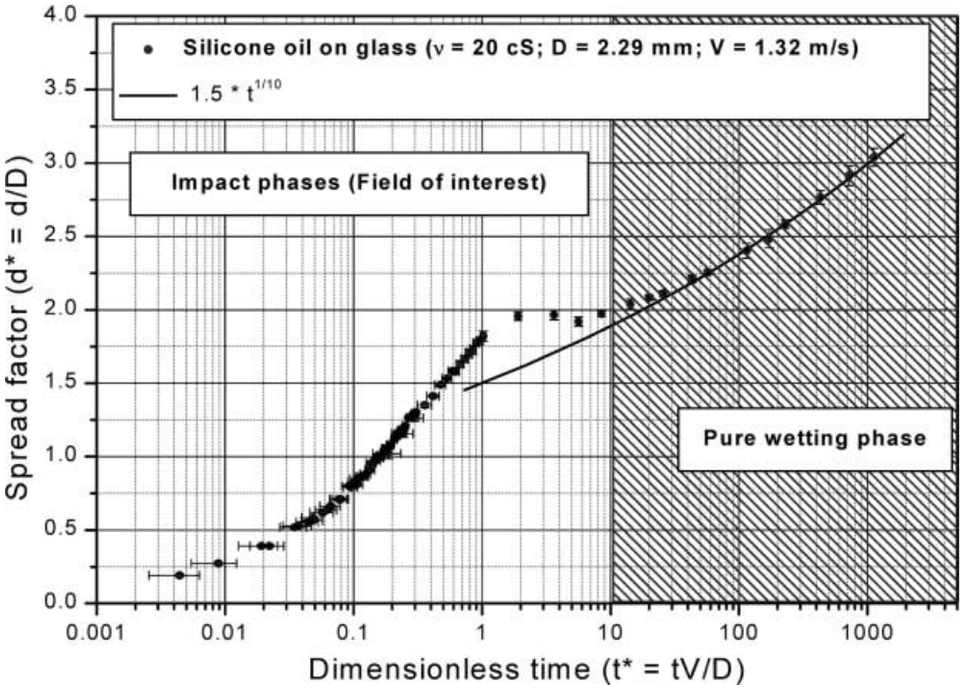

Fig. 15. Spread history for a completely wettable system

the entire impact process ($t^*\subset[10^{-3}; 5.10^3]$: t can reach several seconds in this case) for a completely wettable system. After the spreading phase, the spreading diameter stays constant for some time, after which it continues to spread. The 'plateau' phase duration (during which d is nearly constant) and the moment of continuation depend on the liquid used. Following the plateau phase, there is a pure wetting phase in which the spreading diameter increases proportionally to $t^{1/10}$, as first demonstrated by Tanner (1979). Further references to experiments on spontaneous drop spreading for a completely wettable system can be found in Kistler (1993).

4 Discussion

The first stage of spreading exhibits no ejection of the lamella from the body of the drop. However, the shock wave should trigger a lamella ejection at the moment of impact (Engel 1955; Lesser and Field 1983; Field et al. 1985; Dear and Field 1988). The moment of shock wave detachment calculated for impact velocities of a few meters per second is only a few nanoseconds (minimum 0.45 ns for the case of Fig. 4 and 6 ns for the maximum possible value using Lesser and Field's solution; 2.3 ns using Engel's solution). There appear to be two possible explanations why a lamella is not observed in Fig. 3b at t=20 μs (or in any other comparable sequences). First, if a lamella is formed by a shock wave detachment from the solid wall, it would be so thin that even with the image resolution of the present set-up (under 10 μm) no detection is possible. This explanation is improbable. The more likely reason is that the impact velocities in the present experiments are much lower than in previous experiments (Lesser and Field 1983; Field et al. 1985; Dear and Field 1988), and thus the shock wave either does not exist or is much weaker and is dissipated earlier. As a result, it is not sufficient to induce the lamella ejection. The conclusion is therefore that in the present experiments a shock wave does not exist and that the lamella has different physical origins than observed in the earlier work.

In the *kinematic phase*, the contact line movement is determined only by geometric considerations, as explained using Fig. 16. The contact line simply corresponds to the circumference of a horizontal cut through the drop moving with a downward vertical velocity V. Accordingly, the drop spreading diameter can be easily expressed in non-dimensional form as

$$d* = 2\sqrt{t*(1-t*)}.$$

for small t^* this results in a $\sqrt{t*}$ dependence of the spreading diameter, experimentally confirmed with the new results given in Fig. 4. The different numerical coefficient found by fitting the experimental data indicates the uncertainty associated with determining time zero. Such an interpretation also explains why the shape of the droplet upon impact can be very influential during this early spreading stage, as observed in Fig. 7. However, this ad hoc geometric model violates the continuity equation, assuming the fluid is incompressible. A simple calculation shows, however, that even if the volume of fluid "below" the impact surface were uniformly redistributed throughout the drop (Kim et al. 2000), the increase in drop diameter would be negligible and below the present resolution limits of the images. For instance, for t^*=0.05, only a 0.43% diameter increase would be expected.

The kinematic phase ends when material points at the base of the drop start to move radially and not mainly vertically, which corresponds to the generation of a lamella. The sharpness of this deformation is influenced, of course, by the impact velocity. It might be expected that

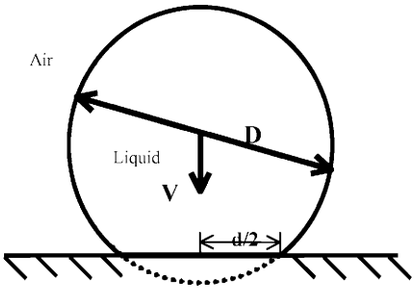

Fig. 16. Movement of the contact line during the kinematic phase

the drop size would also influence this spreading, however, in the present study the drop was always larger than 1.2-mm diameter and no significant influence of drop size could be detected. The present observations confirm that the viscosity is an important influencing parameter throughout the entire spread process (e.g. Fig. 8). Variations of the spread behaviour due to surface tension were only observed at large nondimensional times and were less pronounced. However, it must be kept in mind that while the viscosity could be varied over a factor of 1,000 in this study, the surface tension was only varied by a factor of 3.5. The results shown in Fig. 11 indicate that the Reynolds number and Weber number based on the impact parameters are not adequate to describe the entire impact process. This is because the lamella spreading exhibits different length and velocity scales than the initial drop diameter and velocity. Furthermore, the length and velocity scales governing the spreading lamella change rapidly with time, so that the relative importance of capillary and viscous forces compared with inertial forces also change with time. The phenomenology of the impact varies significantly for different parameters (Fig. 14), therefore it is unlikely that a simplified and universal model can be found for estimating the length and velocity scales appropriate to describe the entire lamella spreading.

The advancing and receding contact angles measured with the sessile drop method define for a given liquid volume a maximum (receding contact angle) and minimum (advancing contact angle) diameter, d_r and d_a, respectively, of the drop in a metastable state, where only evaporation remains an influence (de Gennes 1985). These two diameters d_r, d_a are pictured in Fig. 14a. If the droplet shape is approximated as a truncated spherical cap, these two diameters are given by

$$\frac{d_r}{D} = 2\left[\frac{\sin^3\theta_{rec}}{2(1-\cos\theta_{rec})(2-\cos\theta_{rec}-\cos^2\theta_{rec})}\right]^{1/3},$$

$$\frac{d_a}{D} = 2\left[\frac{\sin^3\theta_{adv}}{2(1-\cos\theta_{adv})(2-\cos\theta_{adv}-cos^2\theta_{adv})}\right]^{1/3}.$$

This approximation should be valid when the length scales of the problem are smaller than the Laplace length $a = \sqrt{\sigma/\rho g}$. This is always the case in these experiments since $1.5\times10^{-3}<a$ [m]$<2.7\times10^{-3}$. In addition, the last photographs in Fig. 13b, d indicate that this approximation is realistic.

The receding diameter d_r will always be larger than the advancing diameter d_a, as indicated in the sketch shown in Fig. 14. Thus, depending on the impact conditions (impact velocity and drop diameter) and the ratio of the maximum achieved spreading diameter to the diameters d_r and d_a, the contact line will advance or recede. For example, for a very low wettable system (θ_{adv}=95, θ_{rec}=90) and with a very viscous liquid drop impacting at low velocity, the inertia will be low compared with viscous effects (low Reynolds number). The viscous effects will dissipate most of the available kinetic energy and the drop will just attain the advancing diameter d_a. In the case of higher inertia, the spreading diameter will overshoot the advancing diameter d_a up to a position lying between the advancing and receding diameters or will even exceed the receding diameter d_r. If the receding diameter is exceeded, then the drop will begin to recoil. If the receding motion is slow enough, the diameter will remain at the receding diameter value. At higher receding velocities it will pass through the value of the receding diameter to finalise at a value between the two diameters. It is possible to imagine a case of a small hysteresis and low viscosity where the diameter would even oscillate around the two diameters d_r and d_a, and finally stabilise between them.

This concept of the dependence of impact outcome on the comparison between the maximum spreading diameter and the advancing and receding equilibrium diameters is tested in Fig. 14 by calculating d_r and d_a for several of the test conditions The bars shown on the right side of the diagram indicate the range defined by the d_r and d_a diameters. (The symbols between the bars indicate the corresponding case). All experimental results are consistent with this model of advancing and receding diameters. This means drops exhibiting a recoil always exceed their corresponding receding diameter, and otherwise the final diameter always lies between the two diameters (within experimental accuracy and provided that no break-up or splash occurred, so that preservation of the drop volume is conserved). Note that this concept of advancing and receding diameters was alluded to in Schiaffino and Sonin (1997), but was not evaluated quantitatively.

Another interesting feature is observed during the receding phase, which occurs for highly nonwettable surfaces. At higher impact velocities, the maximum spreading radius achieved by the expanding lamella is also higher and eventually exceeds the receding diameter. This leads to a receding velocity (by a factor of approximately 2 in these experiments: 0.3 m/s and 0.57 m/s). An increase of the receding velocity enhances the probability of a receding break-up (Rioboo et al. 2001). In the case of a receding break-up, the energy left in the main drop is no longer sufficient to achieve a partial rebound.

The surface roughness always influences the spreading of the contact line. Since the liquid must follow the local surface topology, small irregularities introduce vertical velocity perturbations and thus also increase the dissipated energy. On the other hand, these perturbations are also the direct cause of the prompt splash in the case of high velocity impacts onto rough surfaces. Increasing the amplitude of the roughness will increase the perturbations and also increase the probability of a prompt splash. In the present

experiments the impact on rough wax did not produce a prompt splash, whereas impact on rough glass, with smaller roughness elements, did. This also indicates that the shape of the roughness elements plays a role. The roughness elements on glass were, for instance, more jagged than on wax. This effect has yet to be studied systematically.

For the case of complete wetting, there is no final diameter. The liquid spreads until it reaches the state of a monolayer, governed only by the surface inhomogeneities, be they topological or chemical.

5 Conclusions

The drop impact process onto dry surfaces has been examined for a systematic variation of influencing parameters, including impact velocity, drop diameter, liquid viscosity and surface tension, surface wettability and roughness amplitude and wavelength. The impact has been characterised by the spreading behaviour of the drop, quantified by the spreading diameter over time and by the nature of the final impact outcome.

The impact time evolution can be divided into various phases. The kinematic phase corresponds to the earliest stage of impact, when no noticeable lamella propagates radially from the base of the drop. During this phase, similarity is obtained over all experimental conditions examined, with a simple scaling according to drop impact velocity and initial diameter. The appearance of the lamella cannot be explained in terms of a shock wave detachment upon impact. Only after the kinematic phase do the various material and dynamic parameters of impact begin to influence the spreading process. However, it has been shown that the Reynolds and Weber numbers based on primary drop parameters are not sufficient to capture all of the observed effects. For further discussion on this point see Roisman et al. (2002).

For the various phases of the process, the different influencing parameters change in their importance, i.e. the dimensionless numbers to be taken into account vary throughout the spreading evolution. Until the moment the lamella's diameter reaches its maximum or the plateau phase, the spreading diameter is decelerating.

The maximum spreading diameter has a meaning only relevant for the case of nonwettable systems. The roughness has an immediate influence on the probability of prompt splash. The comparison of different roughness suggests that an even more detailed specification of the roughness, other than a simple standard deviation of the height, will be necessary. The wettability has a profound influence on the final outcome of the impact, in particular the nonwettable systems result in a receding phase and, under some conditions, a receding break-up. A quantitative measure of these wettability effects requires additional parameters such as the advancing and receding dynamic contact angles.

References

Cheng L (1977) Dynamic spreading of drops impacting onto solid surfaces. Ind Eng Chem Proc Des Dev 16:192–197

Dear JP, Field JE (1988) High-speed photography of surface geometry effects in liquid/solid impact. J Appl Phys 63:1015–1021

de Gennes PG (1985) Wetting: statics and dynamics. Rev Mod Phys 57:827–863

Engel O (1955) A water drop collision with solid surfaces. PJ Res Nat Bur Stand 54:281–298

Field JE, Lesser MB, Dear JP (1985) Studies of two-dimensional liquid wedge impact and their relevance to liquid-drop impact problems. Proc R Soc London A 401:225–249

Frohn A, Roth N (2000) Dynamics of drops. Springer, Heidelberg, Berlin

Fukai J, Shiiba Y, Yamamoto T, Mitayake O, Poulikakos D, Megaridis CM, Zhao Z (1995) Wetting: effects on the spreading of a liquid droplet colliding with a flat surface: experiments and modeling. Phys Fluids A 7:236–247

Hartley GS, Brunskill RT (1958) Reflection of water drop from surfaces. In: Surface phenomena in chemistry and biology. Pergamon, Oxford, pp 214–223

Hoffman RL (1975) A study of the advancing interface. 1. Interface shape in liquid–gas systems. J Colloid Interface Sci 50:228–241

Johnson RE, Dettre RH (1993) Wetting of low-energy surfaces. In: Berg JC (ed) Wettability. Dekker, New York, pp 1–73

Kim HY, Feng ZC, Crun JH (2000) Instability of a liquid jet emerging from a droplet upon collision with a solid surface. Phys Fluids 12:531–541

Kistler SF (1993) Hydrodynamic of wetting. In: Berg JC (ed) Wettability. Dekker, New York, pp 311–349

Lesser MB, Field JE (1983) The impact of compressible liquids. Ann Rev Fluid Mech 15:97–122

Levin Z, Hobbs PV (1971) Splashing of water drops on solid and wetted surfaces: hydrodynamics and charge separation. Phil R Soc London A 269:555–585

Mao T, Kuhn DCS, Tran H (1997) Spread and rebound of liquid droplets upon impact on flat surfaces. AIChE J 43:2169–2179

Middleman S (1995) Modelling axisymmetric flows. Academic, London

Mourougou-Candoni N, Prunet-Foch B, Legay F, Vignes-Adler M, Wong K (1997) Influence of dynamic surface tension on the spreading of surfactant solution droplets impacting onto a low surface energy solid substrate. J Colloid Interface Sci 192:129–147

Onda T, Shibuichi S, Satoh N, Tsujii K (1996) Super water repellent fractal surfaces. Langmuir 12:2125–2127

Podvysotskii AM, Shraiber AA (1993) Experimental investigation of mass and momentum transfer in drop-wall interaction. Izv Mekh 2:203–208

Prunet-Foch B, Legay F, Vignes-Adler M, Delmotte C (1998) Impacting emulsion drop on a steel plate: influence of the solid substrate. J Colloid Interface Sci 199:151–168

Range K (1995) Impact, étalement et éclatement de gouttes sur diverses surfaces horizontales ou inclinées. PhD thesis, University of Paris 6

Richard D (2000) Situations de mouillage nul. PhD thesis, University of Paris 6

Rioboo R, Marengo M, Tropea C (2001) Outcomes from a drop impact on solid surfaces. Atomization Sprays 11:155–166

Roisman IV, Rioboo R, Tropea C (2002) Normal impact of a liquid drop on a dry surface: model for spreading and receding. Proc R Soc London A (in press)

Schiaffino S, Sonin AA (1997) Molten droplet deposition and solidification at low Weber numbers. Phys Fluids A 9:3172–3187

Stow CD, Hadfield MG (1981) An experimental investigation of fluid flow resulting from the impact of a water drop with an unyielding dry surface. Proc R Soc London A 373:419–441

Tanner LH (1979) The spreading of silicone oil drops on solid surfaces. J Phys D 12:1473–1484

Worthington AM (1877a) On the forms assumed by drops of liquids falling vertically on a horizontal plate. Proc R Soc London 25:261–271

Worthington AM (1877b) A second paper on the forms assumed by drops of liquids falling vertically on a horizontal plate. Proc R Soc London 25:498–503

Zhang X, Basaran OA (1997) Dynamic surface tension effects in impact of a drop with a solid surface. J Colloid Interface Sci 187:166–178